

The C-flash and the ignition conditions of type Ia supernovae

P. Lesaffre,^{1,2*} Z. Han,³ C. A. Tout,^{1,4} Ph. Podsiadlowski² and R. G. Martin¹

¹*Institute of Astronomy, Madingley Road, Cambridge CB3 0HA, UK*

²*University of Oxford, Department of Astrophysics, Oxford OX1 3RH, UK*

³*National Astronomical Observatories/Yunnan Observatory, the Chinese Academy of Science, PO Box 110, Kunming 650011, China*

⁴*Centre for Stellar and Planetary Astrophysics, School of Mathematics, Monash University, Clayton, Victoria 3800, Australia*

Received September 15, 1996; Accepted March 16, 1997

ABSTRACT

Thanks to a stellar evolution code able to compute through the C-flash we link the binary population synthesis of single degenerate progenitors of type Ia supernovae (SNe Ia) to their physical condition at the time of ignition. We show that there is a large range of possible ignition densities and we detail how their probability distribution depends on the accretion properties. The low density peak of this distribution qualitatively reminds of the clustering of the luminosities of Branch-normal SNe Ia. We tighten the possible range of initial physical conditions for explosion models: they form a one-parameter family, independent of the metallicity. We discuss how these results may be modified if we were to relax our hypothesis of a permanent Hachisu wind or if we were to include electron captures.

Key words: – supernovae: Type Ia – white dwarfs

1 INTRODUCTION

Phillips relations (Phillips 1993) have made type Ia supernovae (SNe Ia) a very useful tool for cosmology. The correlation between their absolute peak brightness (M_{peak}) and their decline rate (Δm_{15}) has been used to infer distances of high redshift galaxies and refine our knowledge of cosmological parameters (e.g. Tonry et al. 2001). However current models are not able to reproduce the range of Δm_{15} observed: we still do not understand what primary parameter is responsible for the main diversity of SNe Ia. Moreover there exists a finite spread of M_{peak} for a given Δm_{15} which hints at the existence of a secondary parameter. Knowledge of both these controlling parameters could help remove any bias from cosmological measurements due to an evolution of the secondary parameter and help reduce the scatter of the Phillips relation.

With synthetic light curves and spectra with explosion models, attempts have been made to infer what parameters of the explosion control which observational property (Röpke & Hillebrandt 2004, for example). In this paper we proceed from the binary population synthesis of SNe Ia progenitors where we only consider the single degenerate channel, one of the most promising channels for the progenitors of SNe Ia. We model their evolution until we get the physical conditions at the time of the ignition. We start our com-

putations just after a white dwarf (WD) has been formed through a common envelope evolution phase. The initial parameters are the WD composition, its initial mass M_{WD}^1 , the initial mass M_2^2 of the secondary and the initial separation a_i . The WD cools down while the secondary evolves until it overflows its Roche lobe at the end of its main-sequence evolution (cooling phase). Accretion on to the WD heats it up and enhances its central density until the carbon fusion starts (beginning of the accretion phase). The rate of energy production due to burning and accretion soon overcomes the losses due to escaping neutrinos and photons: thermal balance does not hold anymore (birth of the convective core). However, the high electron degeneracy and the high temperature sensitivity of the burning rate prevent expansion from controlling the burning and the convective core has to grow very fast to cope with the increasing energy generation rate: a flash ensues (C-flash phase). Convective flows are able to get rid of the energy released by carbon burning until the turnover time scales become too long relative to the heating rate. At this point it is believed that one or multiple bubbles ignite and a flame front propagates out and eventually unbinds the star (ignition or beginning of the explosion). In the present work we investigate the probability distributions and correlations between various characteristics of the star at the time of ignition which are thought to influence the outcome of the explosion.

Section 2 presents the details of our numerical setup and the main grid of models. In section 3 we describe the result-

* lesaffre@ast.cam.ac.uk

ing ignition conditions. In sections 4 and 5 we investigate the role of metallicity and the effects of binary evolution respectively. And in sections 6 and 7 we discuss and summarise our results.

2 METHOD

2.1 Stellar evolution code

We improved the Eggleton code (Eggleton 1971; Pols et al. 1995) to enable the modelling of white dwarfs from their cooling tracks and the start of the accretion to the very late phases of the C-flash until shortly before the explosion takes place. Note that neutrino losses in the Eggleton code are from Itoh et al. (1992): they are an important factor that determine the position of the central density-temperature tracks of the WD.

We consider only the $^{12}\text{C}+^{12}\text{C}$ fusion reaction and assume that ^{24}Mg is its only product. We hence completely neglect all nucleosynthesis issues such as Urca processes which are likely to occur during the C-flash (see Lesaffre et al. 2005).

For each chemical species described in the code we solve not only for its mass fraction but also for its spatial gradient. This allows us to compute the mixing for realistic diffusion time scales as given by the mixing length theory (MLT). This is important because close to ignition convective turnover time scales become comparable and even longer than the burning time scales.

We compute the equations of hydrostatic stellar evolution on a staggered mesh which allows us to take arbitrarily small time steps required by the burning time scales. This is also needed to stabilise chemical equations including both gradients and composition. Radius, mass, luminosity and chemical gradients are hence computed on the interfaces of the computational shells whereas all other variables are taken at the centre of mass of each zone.

We make use of a moving grid algorithm (Dorfi & Drury 1987; Lesaffre et al. 2004a) with a time delay of one year. This friction of the grid limits numerical diffusion and appears to stabilise the code against rapid changes at the onset of accretion and near ignition.

Last but not least we implemented a scheme to track the boundaries of convective regions within a zone. As the time scale for burning decreases, a discrepancy builds up between the rate of change of temperature within and outside the convective core. When convective boundaries are tied up to the interfaces of the computational zones, the code has more and more difficulty to converge and breaks down way before the explosion takes place. We need to release the convective boundaries and interpolate the convective criterion¹ to infer their position inside a zone. We are then able to account properly for the discontinuity in the rate of change of temperature. Chemical rates of change benefit from exactly the same treatment but chemical profiles are discontinuous at convective frontiers (unlike the temperature) and they require an additional flux through the advancing boundary of the core.

¹ We use the Schwarzschild criterion without overshooting

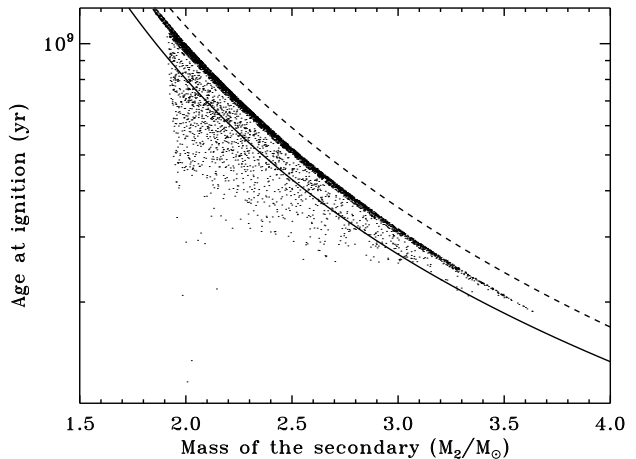


Figure 1. Age vs. mass of the secondary for our sample of type Ia progenitors. The solid and dashed lines are analytical estimates for the age of the main sequence taken from Eggleton et al. (1989) (solid) and Hurley et al. (2000) (dashed).

2.2 Initial WD models

We build a series of WD models of different masses M_{WD}^i by accreting on a very low-mass ($0.3 M_{\odot}$) C+O WD model at a rate of $10^{-7} M_{\odot}/\text{yr}$ which mimics the growth of the CO core during the giant branch evolution. This gives a very crude estimate for the thermal state of the WD when it is first formed. This is however not essential as the thermal profile relaxes during the subsequent cooling phase. Umeda et al. (1999a) and Domínguez et al. (2001) have shown how the mass and metallicity of the progenitor star of the WD influence its chemical state. In the present study we use their results to build synthetic chemical profiles of the initial white dwarf. We use their central values for the C/O ratio (linearly interpolated at M_{WD}^i) to build a central core of mass half the white dwarf. This is then connected linearly to a C/O ratio of 1 uniform in the outermost 10% in mass of the WD.

2.3 Cooling phase

The newly formed WD cools down at constant mass until the secondary star fills its Roche lobe, which generally happens at the end of its main sequence, on its way to become a giant (in the Hertzsprung gap) or on the giant branch. In each case the cooling time is close to the main-sequence age of the secondary star (see figure 1). For a given WD mass the length of the cooling phase generally determines the temperature at its centre. It does not depend much on its initial thermal profile. Hence the initial conditions for the accretion phase depend only on the age of the secondary and the mass of the WD.

2.4 Accretion phase

When the secondary starts to overflow its Roche lobe it transfers mass on to the WD. How fast an accretion rate the WD can cope with is a crucial question and is still the object of much debate. In this study we follow Han & Podsiadlowski (2004) and assume that the Hachisu

wind model (Hachisu et al. 1996) holds. The WD accommodates high mass transfer rates by getting rid of the extra mass through a wind as long as the mass transfer rate exceeds a critical rate \dot{M}_{cr} given by

$$\dot{M}_{\text{cr}} = 5.3 \times 10^{-7} \frac{(1.7 - X)}{X} (M_{\text{WD}}/M_{\odot} - 0.4) M_{\odot} \text{ yr}^{-1} \quad (1)$$

where $X = 0.7$ is the hydrogen mass fraction in the accreted material from the secondary and M_{WD} is the mass of the WD. As a further simplification we assume that the mass transfer rate is *always* higher than this critical rate so that the Hachisu wind determines the accretion rate on to the WD. The net growth of the C+O WD is finally modulated by the efficiency of He-shell flashes according to

$$\dot{M}_{\text{WD}} = \eta_{\text{He}}(\dot{M}_{\text{cr}}) \times \dot{M}_{\text{cr}} \quad (2)$$

where η_{He} is given by equation (4) of Han & Podsiadlowski (2004). With these assumptions the growth rate of the WD depends only on the mass of the WD. We estimate the effects of the end of the wind phase in section 5.

2.5 Ignition

When convection is no longer able to evacuate the energy input from the C-burning, thermal runaway starts in some bubbles near the centre and the star explodes. Exactly how and when this occurs is still unclear but recent developments allow us to pinpoint analytic conditions for the ignition of the flame (Woosley et al. 2004; Wunsch & Woosley 2004). Here, we stop our computation when the differential burning time scale t_{b} is shorter by a given fraction α of the local convective turnover time scale t_{c} at some point in the star. Here t_{b} is the e-folding time scale of a temperature fluctuation subject to C-burning:

$$t_{\text{b}}^{-1} = \frac{1}{c_{\text{P}} T} \left. \frac{\partial q}{\partial \ln T} \right|_{\rho}, \quad (3)$$

where T is the temperature, ρ is the mass density, c_{P} is the specific heat at constant pressure and q is the rate of energy generation due to C-burning and t_{c} is a convective element's crossing time over a pressure scale height:

$$t_{\text{c}} = \frac{H_{\text{P}}}{u_{\text{c}}}, \quad (4)$$

where H_{P} is the pressure scale height and u_{c} is the convective velocity as given by MLT.

When $t_{\text{b}} = t_{\text{c}}$ ($\alpha = 1$) the differential burning time scale is of the same order as the convective turnover time scale. At this point differential reactivity (the fact that upward and downward moving fluid elements burn at different rates) should be included in the treatment of convection to get accurate mixing and temperature excesses (see Lesaffre et al. 2005, 2004b).

In our models (in which we use classical MLT) it turns out that the temperature excess is typically 0.025% when this happens. It takes roughly eight e-foldings to grow from 0.025% to 100%. Hence can we estimate that temperature fluctuations will be big for $t_{\text{b}} = t_{\text{c}}/8$ ($\alpha = 1/8$). At this point, a typical ascending temperature fluctuation increases its temperature up to twice the average temperature before it is mixed. We take this as a plausible point for the start of the thermal runaway.

Wunsch & Woosley (2004) consider a temperature background fixed in time and analyse the growth of perturbations relative to this background. As a result they find that the relevant time scale for the growth of the temperature fluctuations is the e-folding time scale for the overall burning rate

$$t_{\text{B}}^{-1} = \frac{q}{c_{\text{P}} T}. \quad (5)$$

Because of the high power exponent in the temperature dependence of the burning rate $t_{\text{b}} \simeq t_{\text{B}}/22$. Hence in this picture $\alpha = 1/22$ is a more relevant requirement for the start of the explosion. Note that t_{B} also indicates the time scale of variation for the average temperature in the centre of the star. When $t_{\text{B}} < t_{\text{c}}$ a time-dependent convective model should be used because the turnover time scales become longer than the global evolutionary time scales.

To account for the uncertainty in what determines the start of the explosion, we record models when $\alpha=1, 1/8$ and $1/22$ as possible times for the start of the explosion. In practice all our simulations reach the $\alpha = 1$ point, half of them reach $\alpha = 1/8$ but all break down before $\alpha = 1/22$. We hence extrapolate our results from our last converged model to get the conditions for all these different possibilities for the ignition point. In almost all our simulations the criterion for explosion is first fulfilled at the centre because the local convective time scale is longer there. The only exception is for one run which started off-centre carbon burning and the convective zone never reached the centre (its parameters are $t_{\text{a}} = 0.8$ Gyr and $\dot{M}_{\text{WD}}^{\text{i}} = 0.9 M_{\odot}$, the bottom of the convective region is at $0.05 M_{\odot}$ at ignition). We display results for this run only in figure 4 as most of the quantities that take part in the correlations are defined at or relative to the centre.

2.6 Parameter space

Because we always assume a Hachisu wind phase (except in section 5), the entire evolution of the WD is determined by the cooling age and the initial mass of the WD. Starting with a given initial model, we let it cool down for a time t_{a} after which we trigger the accretion rate \dot{M}_{WD} . The beginning of the accretion is smoothed linearly with a short time scale (10^5 yr) to mimic the rise observed in Han & Podsiadlowski (2004). We build a grid of 24 models spanning six different masses M_{WD}^{i} evenly distributed in the range $[0.7, 1.2] \times M_{\odot}$ and $t_{\text{a}}=0.1, 0.2, 0.4$ and 0.8 Gyr. This grid of models is designed to sample the parameter space of SNe Ia progenitors found by Han & Podsiadlowski (2004). The metallicity is $Z = 0.02$ and we use initial C/O ratios from Umeda et al. (1999a) for this metallicity.

3 IGNITION CONDITIONS

Parameters which have been found to influence the explosion outcome are density, temperature, carbon mass fraction and convective properties. We investigate here how they are related to the parameters M_{WD}^{i} and t_{a} .

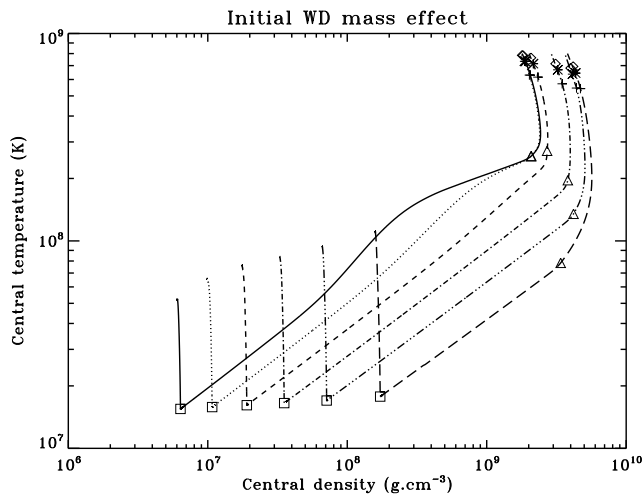


Figure 2. Central density-temperature tracks for different initial WD masses (from left to right: 0.7, 0.8, 0.9, 1.0, 1.1 and 1.2 M_{\odot}) and the same cooling age $t_a = 0.4$ Gyr. Squares, triangles, crosses, stars and diamonds indicate respectively the start of the accretion phase, the growth of the convective core and the $\alpha = 1, 1/8$ and $1/22$ ignition points.

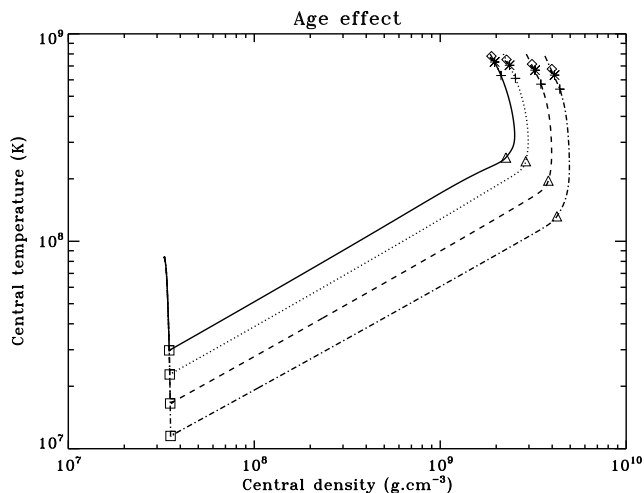


Figure 3. Central density-temperature tracks for different cooling ages (from left to right: 0.1, 0.2, 0.4 and 0.8 Gyr) and the same initial WD mass 1 M_{\odot} . Symbols are as in figure 2

3.1 Central density

Larger initial masses M_{WD}^i yield higher ignition densities because their initial densities are higher (see figure 2). A longer t_a yields a lower initial temperature and a hence higher ignition density (see figure 3).

The dependence of density on M_{WD} and t_a is summarized in figure 4. A WD with a smaller M_{WD}^i has a shorter thermal diffusion time scale and a longer accretion phase. As a result heat waves have time to propagate through the star and the thermal profile of the star reflects the *global* balance between the energy input from the accretion (and burning) and the energy losses from neutrinos. In the rest of the paper we refer to this state as global thermal balance. WDs in a state of global balance all end up on the same ρ_c -

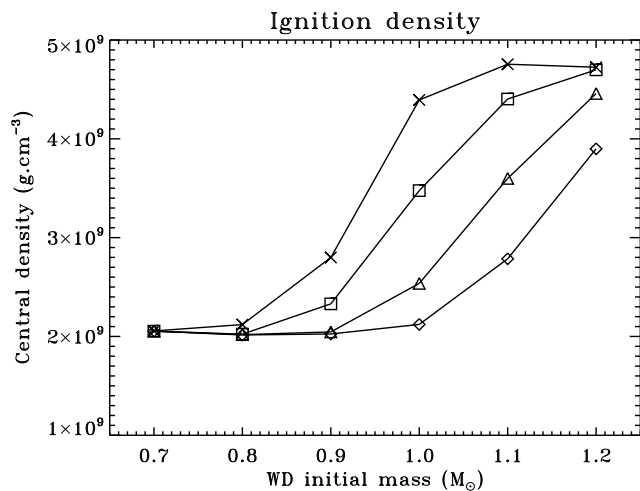


Figure 4. Ignition densities (defined by $\alpha = 1$) vs. initial WD mass for different cooling ages $t_a = 10^8$ yr (diamonds), $t_a = 0.2$ Gyr (triangles), $t_a = 0.4$ Gyr (squares) and $t_a = 0.8$ Gyr (crosses). Densities are only slightly lower for other values of α .

T_c track because the accretion rate depends only on M_{WD} . As a result, they all have the same ignition density. This is reflected in the distribution of ignition densities which has a spike at the lowest density.

Densities also seem to all converge towards the same maximum density for higher initial masses M_{WD}^i . This is due to the shape of the ignition curve which is almost vertical in the $\rho - T$ plane because electron screening enhances C-burning at high density. As a result, the $\rho_c - T_c$ tracks that go to high densities tend to all start the C-flash phase at the same density. Note also that these high densities point towards the importance of electron captures, not yet included in this study.

Ignition density is the parameter that varies most along our grid of parameters. We shall show that most of the other physical properties at ignition are well correlated with this parameter.

3.2 Ignition Temperature

A lower α yields hotter and only slightly less dense ignition conditions because matter is still degenerate at this point. We now examine how the temperature varies according to density when we define the ignition conditions following a given α .

The convective turnover time scale t_c is rather independent of any other parameter at the time of ignition as shown in section 3.3. By contrast the electron screening corrections to the rate of C burning increase it at high density. As a result, because the ignition temperature is defined by the relation $t_b = \alpha t_c$, ignition temperatures are lower for higher densities (see figure 5). This might introduce interesting effects in light of the results of Iapichino et al. (2005) who find a strong sensitivity to the temperature for the properties of igniting bubbles.

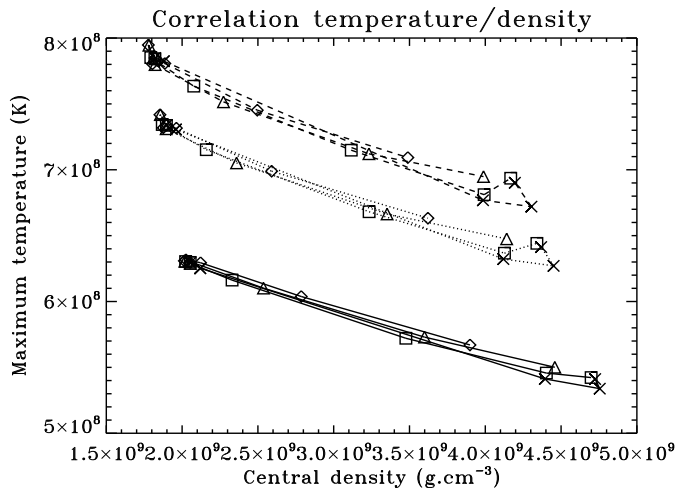


Figure 5. Central temperature vs. central density at ignition central density for $\alpha = 1$ (solid), $1/8$ (dotted) and $1/22$ (dashed). Curves and signs are otherwise labelled as in figure 4.

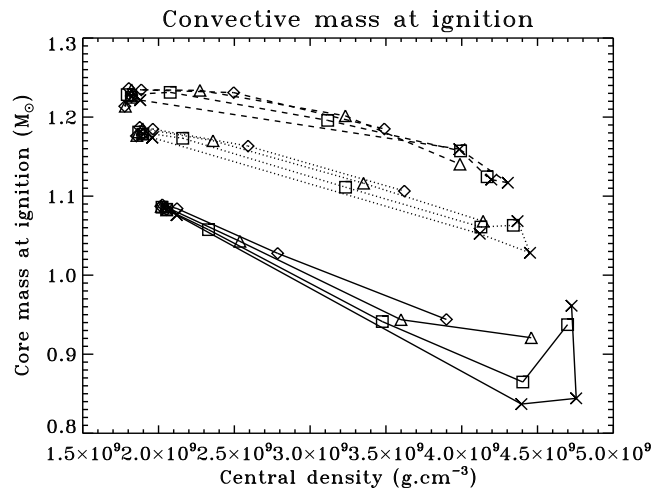


Figure 7. Convective core mass at ignition vs. central density at ignition, labels as in figure 5.

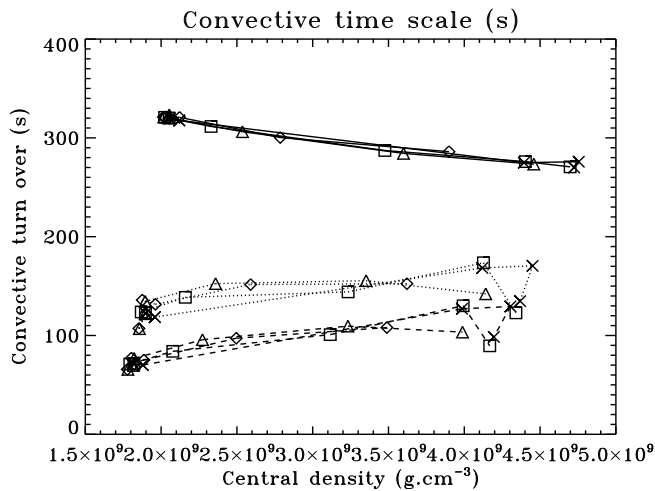


Figure 6. Central convective time scale t_c vs. central density at ignition, labels as in figure 5.

3.3 Convection

Explosion models have recently focused on the importance of the convective state at the beginning of the explosion (Reinecke et al. 2002; Höflich & Stein 2002; García-Senz & Bravo 2005; Wunsch & Woosley 2004). It is interesting to note that our simulations (based on MLT) show very little variation for the convective state at the time of ignition. The turnover time scale t_c appears to be more or less independent of t_a and M_{WD}^i . Naturally these time scales depend upon our definition for the ignition as t_c directly enters our criterion (see figure 6). We recover values in the range 10-100 s as quoted by Wunsch & Woosley (2004) when we use $\alpha = 1/22$. Also worth noting is a weak dependence of t_c on central density. This could be enhanced by convective Urca processes due to the feedback of electron captures on convective velocities (see Lesaffre et al. 2005). The convective core mass at ignition is mainly deter-

mined by the central density which sets the pressure–mass profile and the central temperature which determines the extent of the convective core in the temperature–pressure profile. It is hence not surprising that we recover the same kind of correlations as for the central temperature (see figure 7). We investigate this parameter in light of the rotating progenitor models computed by Yoon & Langer (2004) who found super-Chandrasekhar solutions with a strongly differentially rotating layer around the mass shells $m = 1.1 M_{\odot}$ to $m = 1.25 M_{\odot}$. If the convective core is able to reach this shell before ignition, it might suppress the centrifugal support and leave a higher than Chandrasekhar mass object which may then collapse instead of exploding. On the other hand convective instability might be suppressed by differential rotation and that would trigger the thermonuclear runaway sooner. Figure 7 suggests that the convective core may sometimes reach the differentially rotating layer, depending on what definition we use for the ignition point.

3.4 Carbon mass fraction

The evolution of the central carbon mass fraction is mainly driven by the growth of the convective core which mixes material richer in carbon at a higher rate than the carbon is consumed at the centre. As a result the final carbon mass fraction depends essentially on the composition profile and the initial mass of the WD, that is on the initial M_{WD}^i (see figure 8). The fact that there is little variation among different WDs and the recent result that the explosion might be less sensitive than we think to this parameter (Röpke & Hillebrandt 2004) lead us to conclude that this might not be an essential parameter for understanding the observational properties of SNe Ia. However it is the only parameter that slightly decouples from the central density.

3.5 Magnesium mass fraction

Thanks to our oversimplified treatment of C-burning, the ^{24}Mg mass fraction represents the amount of carbon burnt during the C-flash. We show that this is weakly dependent

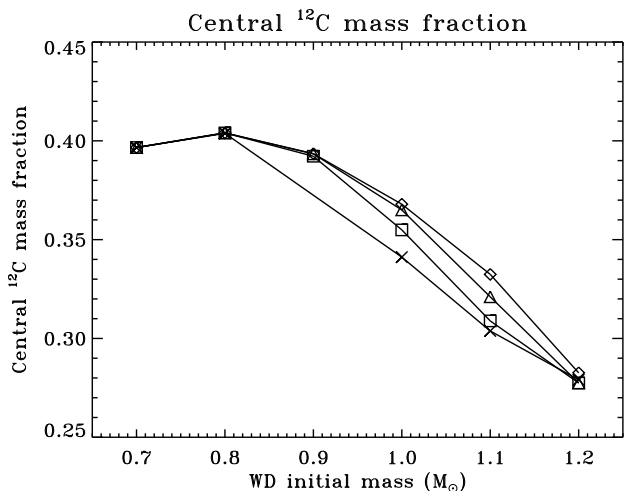


Figure 8. Carbon central mass fraction at ignition vs. initial WD mass, labels as in figure 4.

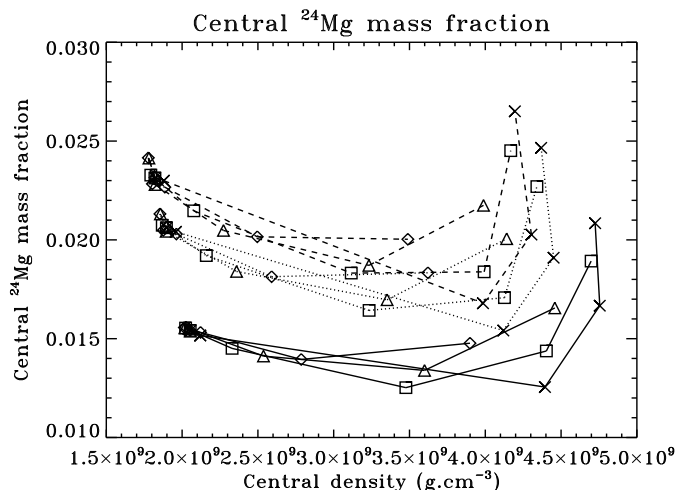


Figure 9. Correlation between Magnesium mass fraction and central density at ignition, labels as in figure 5.

on the central density even though the trend is not clear at high densities (see figure 9). Later ignition (lower α) naturally burns more carbon. The amount of carbon burnt is of interest with regard to Urca species which are among the products of C-burning (^{23}Na and ^{25}Mg , for example).

3.6 Distributions

We use the results of a binary population synthesis that produced 5576 SNe Ia progenitors out of 10^7 initial systems with $\alpha_{\text{CE}} = \alpha_{\text{th}} = 1$ (see Han & Podsiadlowski 2004, section 4). Note that the WD+red giant branch channel is not included in their study: this may affect the distributions. We take the age when the WD reaches the Chandrasekhar mass and the initial mass of the WD as parameters (t_a, M_{WD}^i) which we interpolate linearly on our grid of models to get the central ignition density ρ_i for each of these systems. We display the histogram of ρ_i in figure 10.

The very sharp peak at the lowest density reflects the

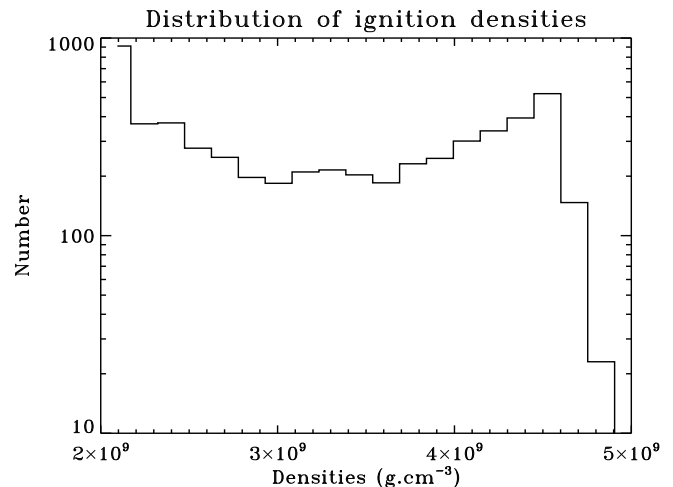


Figure 10. Histogram of the central density at ignition for our 5576 SNe Ia progenitors.

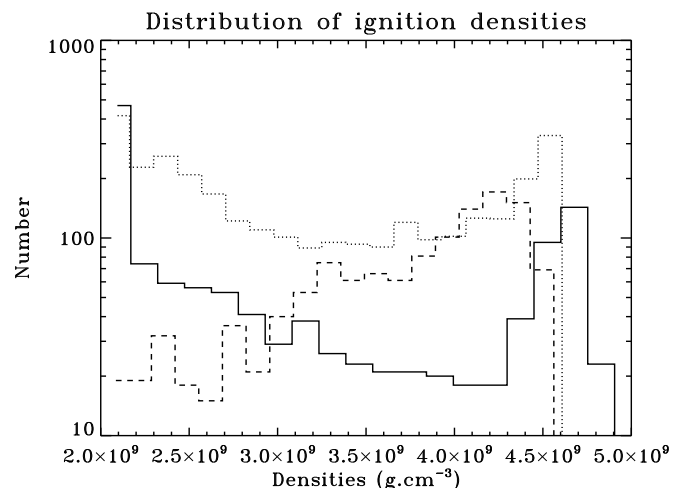


Figure 11. Histogram of the central density at ignition for ages greater than 0.8 Gyr (solid), ages between 0.4 and 0.8 Gyr (dotted) and ages lower than 0.4 Gyr (dashed).

fact that accretion proceeds on longer than thermal diffusion time scales for the lowest initial masses M_{WD}^i . The secondary peak at high density reflects the shape of the ignition curve due to electron screening at high density. It is tempting to associate each one of these peaks to the clustering of either Branch-normal SNe Ia or 91bg like events. But computations of the outcome of the explosions for each of our models need to be performed before we can assess the relation between ignition densities and observational properties of the explosion. The shape of the distribution of M_{WD}^i is rather flat and does not influence the overall probability distribution of ρ_i . However, as noticed by Han & Podsiadlowski (2004), M_{WD}^i is slightly correlated with t_a with lower ages giving rise to higher WD masses on average. As a result more relative weight is given to the high density peak for younger systems (see figure 11).

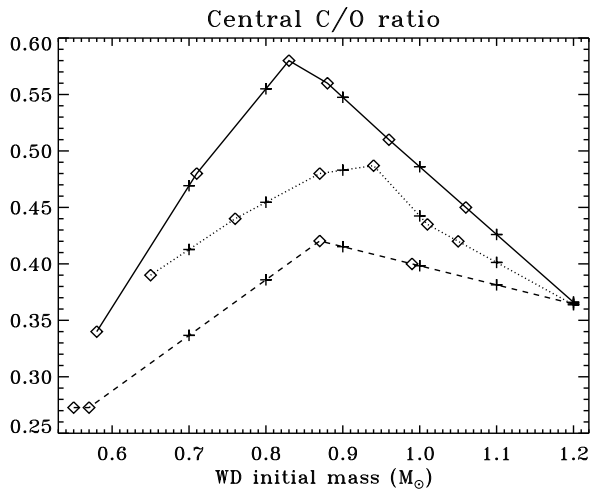


Figure 12. C/O ratio for Umeda et al. (1999a), $Z = 0.02$ (solid) and $Z=0.001$ (dotted) and for Domínguez et al. (2001), $Z=0.02$ (dashed). Diamonds are the values computed by these authors, '+' signs are our interpolated values to compute the initial models.

4 COMPOSITION EFFECTS

In this section we discuss the effects of the composition of the white dwarfs. The initial mass and initial metallicity of their progenitors can vary independently but there can be a correlation between initial mass of the progenitor and that of the white dwarf at the end of the cooling phase.

4.1 Initial C/O ratio

In the previous section all our results are based on central C/O ratios taken from Umeda et al. (1999a). However Domínguez et al. (2001) have found significantly different values for the same solar metallicity as shown in figure 12. This is probably due to their use of different $^{12}\text{C}(\alpha, \gamma)^{16}\text{O}$ reaction rates with Umeda et al. (1999a) using 1.5 times the rate of Caughlan & Fowler (1988) whereas Domínguez et al. (2001) use a higher rate given by Caughlan et al. (1985). We compute here a grid of models using central C/O values from Domínguez et al. (2001) for a fixed cooling age of $t_a = 0.4$ Gyr and the same range of initial masses as previously.

The resulting physical conditions at ignition are virtually identical to the runs described in the previous section. The only slight change is for the central carbon mass fraction which changes as shown in figure 13. This change only reflects the mixing in the convective core of the initial composition profile with the accreted matter.

4.2 Metallicity effects

As shown in figures 12 and 13 a change in metallicity is very much like a change in the initial C/O ratio, except that the magnitude of the effect is even less. In this respect, the metallicity effects can be strictly decoupled from the evolution in the C-flash and computed as in Timmes et al. (2003). However, as noted by Lesaffre et al. (2005), electron captures could change the neutronisation in the course of the

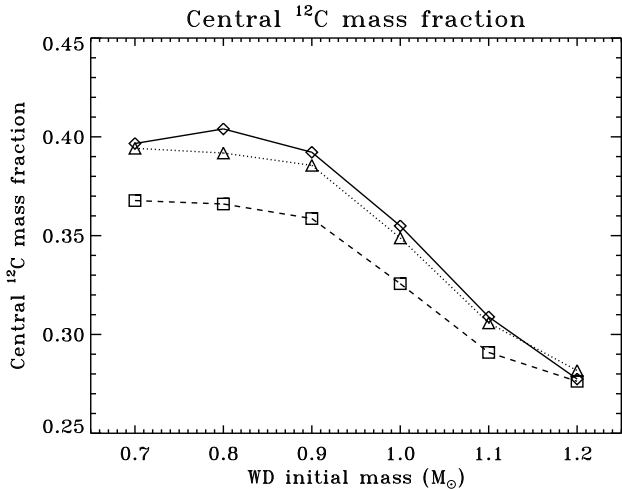


Figure 13. Central carbon mass fraction at ignition for each initial model of figure 12. Diamonds (solid line) are our reference run (see figure 8), triangles (dotted line) are for $Z=0.001$ (Umeda et al. 1999a) and squares (dashed line) are $Z=0.02$ (Domínguez et al. 2001).

C-flash. Whether or not the initial amount of ^{22}Ne has an effect on the detailed nucleosynthesis during the C-flash can be addressed with a more extensive nuclear network than used in this study.

5 BINARY EVOLUTION EFFECTS

The results of previous sections strongly rely on the assumption of a permanent Hachisu wind, which allows us to neglect the binary evolution during the accretion process. Here we examine the effect of varying the accretion rate history.

5.1 End of the wind phase

From figure 1 of Han & Podsiadlowski (2004) we find that the mass transfer rate decays exponentially after the wind has stopped. We hence model the mass transfer rate as

$$\dot{M} = \dot{M}_{\text{cr}}(M_0) - \frac{M_{\text{WD}} - M_0}{t_0} \quad (6)$$

where M_0 is the mass of the WD when the wind stops and t_0 is the time scale for the decay. The value of t_0 varies from 2.7×10^5 yr to 9×10^5 yr in different panels of figure 1 of Han & Podsiadlowski (2004) and we take 6×10^5 yr as a characteristic value. We then use $\dot{M}_{\text{WD}} = \eta_{\text{He}} \dot{M}$.

For three different masses $M_{\text{WD}}^i = 0.8, 1.0$ and $1.2 M_{\odot}$ and $t_a = 0.8$ Gyr we compute the evolution after the end of the wind phase for $M_0 = 1.1, 1.2$ and $1.3 M_{\odot}$ (except for $M_{\text{WD}}^i = 1.2 M_{\odot}$ for which $M_0 = 1.25, 1.3$ and $1.35 M_{\odot}$). Only the central density and the convective core mass at ignition are found to change significantly compared to the models of section 2.

Figure 14 sums up the results for the $\rho_c - T_c$ tracks. The slope of a given track in the $\rho_c - T_c$ diagram depends on the ratio of the rate of change of density and temperature. For a degenerate WD the density is directly linked to the total mass and hence the central density reacts immediately to

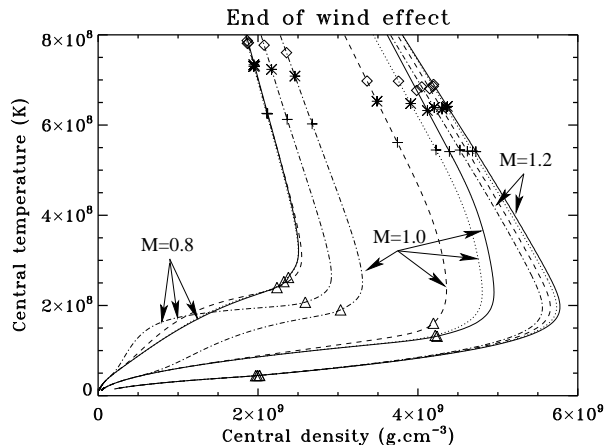


Figure 14. Central density-temperature evolution for three different initial WD masses: 0.8 (left), 1.0 (middle) and 1.2 M_{\odot} (right). Solid lines are the reference runs with a Hachisu wind always on. Other lines stop the wind when the mass reaches three different critical values of M_0 (see text). Labels are dotted, dashed and dash-dotted for decreasing values of M_0 .

any change in mass. On the other hand, the central temperature reacts to a change in accretion at the edge of the WD with a delay of the order of the thermal diffusion time scale t_d across the WD. When the accretion rate slows down, the rate of change of the central density slows down immediately while the temperature continues to increase at the same rate: this steepens the slope of the $\rho_c - T_c$ track. For the lowest masses (left in figure 14), the accretion takes place over a longer time than t_d . Hence global thermal balance is soon reached again and because the accretion rate is smaller this leads to a lower temperature for a given central density. The final result is a slightly higher ignition density. For intermediate masses (middle in figure 14), global thermal balance was not realised at all because the accretion rate was too fast. Hence the temperature was below the temperature the star would reach at global thermal balance. Slowing down the rate now gives time for the star to adjust and its temperature increases, which leads to lower central densities at ignition. For the highest masses (right in figure 14), there is not enough time for the star to react: the effects of slowing down the accretion rate do not reach the central thermal state of the star.

A more significant difference exists for the mass of the convective core at the time of ignition. Indeed, the lower accretion rates yield lower temperatures at the edge of the core. Because the outer boundary of the convective core is determined by the point where the inner adiabatic temperature profile meets the outer temperature profile, the convective core is bigger for lower accretion rates at a given central temperature. We find an increase of between 0.05 and 0.2 M_{\odot} in the convective core mass at ignition when the end of the wind phase is modelled.

We also computed the evolution of a WD using $M_0 = 1.12 M_{\odot}$ and $t_0 = 9.15 \times 10^5$ yr which gives a very accurate fit to the mass transfer rate for panel (a) of figure 1 of Han & Podsiadlowski (2004). But modelling the end of the

wind phase actually makes only very little difference in this case due to the low initial mass of the WD (0.75 M_{\odot}). The only significant change was an increase of about 0.07 M_{\odot} in the convective core mass at ignition.

5.2 Varying the critical accretion rate

To account for uncertainties in the critical accretion rate in the Hachisu wind model (see the discussion in Han & Podsiadlowski 2005), we ran the sequence of masses for $t_a = 0.4$ Gyr with twice the value provided by equation (1). The effect turns out to be quite small, with less than a 10% variation. WDs of lowest initial masses have a slightly lower ρ_i because the global thermal balance for a higher energy input rate yields higher temperatures. The effect is reversed at high initial masses because the shorter accretion times leave less time for the star to reach global thermal balance, so that the rise in central temperature is even more delayed and higher densities are reached at ignition.

5.3 Qualitative results

To properly include the end of the wind would require modelling the stellar evolution of the secondary along with the WD. We do not do this explicitly here. However, a decrease of the accretion rate at the end of the wind phase as in section 5.1 mainly lowers the ignition density for WDs of intermediate initial masses. This suggests that binary evolution effects depopulate intermediate ignition densities to the benefit of the lowest densities. Hence the probability distribution function of ignition densities should have a sharper peak at high density and a broader peak at low density. The broadening of the low-density peak would also be emphasised by the slight increase in ρ_i for lowest initial WD masses in systems that terminate their wind early on.

6 DISCUSSION

The main uncertainty in our model comes from the Hachisu wind model (discussed in section 5) but our results seem to hold even for significant variation in the accretion history. In section 4 we showed that, although the initial C/O ratios are not well known, they do not affect our results very much.

The main caveat of our study is that we do not include electron captures while our models go to quite high densities. In the future we hope to be able to include the convective feedback as in Lesaffre et al. (2005) but until now technical difficulties have prevented us (Lesaffre et al. 2004b). If there was indeed a negative feedback on convective velocities, the mixing would be less efficient. Consequently the abundance changes would be enhanced and the explosion would probably take place sooner, at higher densities. In particular electron captures would increase the neutronisation during the C-flash which may have dramatic consequences for the outcome of the explosion (Timmes et al. 2003). Less homogeneous abundance profiles at the time of the explosion may also have consequences for the way the flame propagates because it goes through a medium increasingly concentrated in fresh fuel. Finally electron captures would tend to slightly increase the density compared to our models but this would probably be a small effect.

The high densities encountered in our models raise the question of whether the star will undergo an electron-capture supernova type of event leading to the formation of a neutron star rather than a thermonuclear explosion. However Gutiérrez et al. (2005) indicate that a thermonuclear explosion is very likely given the high C mass fractions in our models.

Accreting WDs are almost certainly strongly rotating. Yoon & Langer (2004) have shown how much influence this could have on the fate of the WD and how this could account for part of the type Ia diversity. However rotation is directly linked to the accretion so that it probably does not generate a new independent parameter. Our study has shown, at least in some cases, that the convective core is likely to reach the strongly differentially rotating region that helps support the star to higher than Chandrasekhar masses. Rotation might then help to increase the influence of binary evolution effects that seem secondary in this study.

Finally this study is valid for the single degenerate channel only. If a Hachisu wind holds as well for the accretion of a WD on to another WD, we may apply part of the results presented here but in this case the C/O ratio of the accreted matter can be different from 1. However the complete disruption of the accreted WD is likely to lead to a picture quite different from the Hachisu wind.

7 CONCLUSIONS

We link the properties of single degenerate type Ia progenitors at the time of the ignition to results of a binary population synthesis thanks to successful models of the C-flash.

We show that there is a large range of possible ignition densities whose distribution reflects the properties of the accretion on to the WD. Furthermore, almost any other property of the WD at the time of the ignition is correlated to the ignition density: this makes it a one parameter family of models which considerably tightens the range of possible initial conditions for explosion models. The convective time scales, amount of C-burning and central temperatures are functions of the central density at ignition. The central C mass fraction is better correlated to the initial mass of the WD progenitor. The core mass at ignition can be modified according to how the mass transfer proceeds (this implies a sensitivity to the initial separation of the binary). These last two parameters may hence be regarded as slightly independent of the ignition densities, although they do not have a large range of variation and are hence probably less essential than the density for the explosion.

We have investigated several criteria that determine when the star would explode. Although the actual dependence on density of the temperature, convective state and amount of C-burning are sensitive to the criterion chosen, we note that their correlations to density are still tight and the distribution of ignition densities does not change.

We show that the metallicity has almost no effect on the C-flash phase. Hence this parameter is independent of the central density at ignition. Because both have been shown to have a big effect on the explosion outcome, we postulate that ignition density and metallicity are the two main parameters responsible for the diversity of type Ia supernovae. Metallicity has a linear effect on the peak bright-

ness of type Ia supernovae with low metallicity yielding brighter M_{peak} (Timmes et al. 2003; Travaglio et al. 2005; Mazzali & Podsiadlowski 2005). However the effect of density on M_{peak} is still unclear: hydrodynamics of the explosion suggest that more mass is burnt to nuclear statistical equilibrium for higher densities but explosion nucleosynthesis (Travaglio et al. 2004) predicts that more stable elements are produced at higher densities because of electron captures.

If density is the primary parameter and metallicity is the secondary parameter, then metallicity changes could shift the Phillips relation. On the other hand if metallicity is the primary parameter and density is the secondary parameter there should be less change in the Phillips relations, unless metallicity strongly affects the M_{WD}^i distribution as postulated by Umeda et al. (1999b). Finally, density and metallicity might be degenerate and both be primary parameters. The chain of computations from the ignition conditions to the light curves via explosion models and explosive nucleosynthesis (including electron captures) must be completed before we can theoretically address the effect of each parameter and uncover the physical nature of the Phillips relation. Observations of correlations with host galaxy metallicities (Gallagher et al. 2005) and comparison of type Ia luminosity functions with the metallicity or ignition density distributions will also give important clues.

ACKNOWLEDGEMENTS

This work was mainly funded through a European Research & Training Network on Type Ia Supernovae (HPRN-CT-20002-00303). It was also supported in part by the Chinese National Science Foundation under Grant Nos. 10521001 and 10433030 (Z.H.).

REFERENCES

- Caughlan G. R., Fowler W. A., Harris, M. J., Zimmerman B. A. 1985, *At. data Nucl. Data Tables* 32, 197
- Caughlan G. R., Fowler W. A. 1988, *At. data Nucl. Data Tables* 40, 283
- Domínguez I., Höflich P., Straniero O. 2001, *ApJ* 557, 279
- Dorfi E. A., Drury L. O'C. 1987, *J. Comput. Phys.* 69, 175
- Eggleton P. P. 1971, *MNRAS* 151, 351
- Eggleton P. P., Tout C. A., Fitchett M. J. 1989, *ApJ* 347, 998
- Eggleton P. P., Fitchett M. J., Tout C. A. 1990, *ApJ* 354, 387
- Gallagher J. S., Garnavich P. M., Berlind P., Challis P., Jha S., Kirshner R. P. 2005, *ApJ* 634, 210
- García-Senz D. Bravo E. 2005, *A&A* 430, 585
- Hachisu I., Kato M., Nomoto K. 1999, *ApJ* 522, 487
- Gutiérrez J., Canal R., García-Berro E. 2005, *A&A* 435, 231
- Han Z., Podsiadlowski Ph. 2004, *MNRAS* 350, 1301
- Han Z., Podsiadlowski Ph. 2005, *MNRAS submitted*
- Höflich P., Stein J. 2002, *ApJ* 568, 779
- Hurley J. R., Pols O. R., Tout C. A. 2000, *MNRAS* 315, 543

- Iapichino L., Brüggem M., Hillebrandt W., Niemeyer J. C.,
A&A accepted
- Itoh N., Mitake S., Iyetomi H., Ichimaru S. 1992, *ApJ* 395,
622
- Lesaffre P., Chièze J.-P., Cabrit S., Pineau des Forêts G.
2004, *A&A* 427, 147
- Lesaffre P., Tout C. A., Stancliffe R. J., Podsiadlowski Ph.
2004, *Memorie della Societa Astronomica Italiana* 75, 660
- Lesaffre P., Podsiadlowski Ph., Tout C. A. 2005, *MNRAS*
356, 131
- Mazzali P., Podsiadlowski Ph., *ApJ submitted*
- Phillips M. M. 1993, *ApJ* 413, L105
- Pols O. R., Tout C. A., Eggleton P. P., Han Z. 1995, *MN-
RAS* 274, 964
- Röpke F., Hillebrandt W. 2004, *A&A* 420, L1
- Reinecke M., Hillebrandt W., Niemeyer J.C. 2002, *A&A*
391, 1167
- Umeda H., Nomoto K., Yamaoka H., Wanao S. 1999, *ApJ*
513, 861
- Umeda H., Nomoto K., Kobayashi C., Hachisu I., Kato M.
1999, *ApJ* 512, L43
- Timmes F. X., Brown E. F., Truran J. W. 2003, *ApJ* 590,
83
- Tonry J., The High-Z Supernova Search Team 2001, *ASPC*
245, 593
- Travaglio C., Hillebrandt W., Reinecke M., Thielemann F.-
K. 2004, *A&A* 425, 1029
- Travaglio C., Hillebrandt W., Reinecke M. 2005, *A&A* 443,
1007
- Woosley S., Wunsch S., Kuhlen M. 2004, *ApJ* 607, 921
- Wunsch S., Woosley S. 2004, *ApJ* 616, 1102
- Yoon S.-C., Langer N. 2005, *A&A* 419, 623